applied sciences

MDPI

Article

Impact of Exhaust Gas Recirculation on Gaseous Emissions of Turbocharged Spark-Ignition Engines

Pedro Piqueras, Joaquín De la Morena *, Enrique José Sanchis and Rafael Pitarch

CMT-Motores Térmicos, Universitat Politècnica de València, Camino de Vera s/n, 46022 Valencia, Spain; pedpicab@mot.upv.es (P.P.); ensanpac@mot.upv.es (E.J.S.); rapiber@mot.upv.es (R.P.)

* Correspondence: joadela@mot.upv.es; Tel.: +34-963-877-650

Received: 5 October 2020; Accepted: 26 October 2020; Published: 29 October 2020

Abstract: Exhaust gas recirculation is one of the technologies that can be used to improve the efficiency of spark-ignition engines. However, apart from fuel consumption reduction, this technology has a significant impact on exhaust gaseous emissions, inducing a significant reduction in nitrogen oxides and an increase in unburned hydrocarbons and carbon monoxide, which can affect operation of the aftertreatment system. In order to evaluate these effects, data extracted from design of experiments done on a multi-cylinder 1.3 L turbocharged spark-ignition engine with variable valve timing and low-pressure exhaust gas recirculation (EGR) are used. The test campaign covers the area of interest for the engine to be used in new-generation hybrid electric platforms. In general, external EGR provides an approximately linear decrease of nitrogen oxides and deterioration of unburned hydrocarbon emissions due to thermal and flame quenching effects. At low load, the impact on emissions is directly linked to actuation of the variable valve timing system due to the interaction of EGR with internal residuals. For the same external EGR rate, running with high valve overlap increases the amount of internal residuals trapped inside the cylinder, slowing down combustion and increasing Unburnt hydrocarbon (HC) emissions. However, low valve overlap (i.e., low internal residuals) operation implies a decrease in oxygen concentration in the exhaust line for the same air–fuel ratio inside the cylinders. At high load, interaction with the variable valve timing system is reduced, and general trends of HC increase and of oxygen and carbon monoxide decrease appear as EGR is introduced. Finally, a simple stoichiometric model evaluates the potential performance of a catalyst targeted for EGR operation. The results highlight that the decrease of nitrogen oxides and oxygen availability together with the increase of unburned hydrocarbons results in a huge reduction of the margin in oxygen availability to achieve a complete oxidation from a theoretical perspective. This implies the need to rely on the oxygen storage capability of the catalyst or the possibility to control at slightly lean conditions, taking advantage of the nitrogen oxide reduction at engine-out with EGR.

Keywords: spark-ignition engines; emissions; fuel consumption; exhaust gas recirculation

1. Introduction

The great majority of research regarding internal combustion engines over the last few decades has been focused on efficiency increase and pollutant emission reduction as a consequence of the progressively more stringent regulations and the need to address the problem of climate change [1]. In this sense, for the last decades, compression ignition engines (CI) have shown important benefits in terms of fuel consumption compared to spark-ignition (SI), whereas the control of exhaust gas emissions requires more expensive and complex aftertreatment systems [2,3]. Therefore, new technologies arised in spark-ignition engines to help reduce the gap in fuel consumption while maintaining the advantages in exhaust emissions [4].

These new technologies such as direct injection, turbocharging and downsizing, variable valvetrain, or exhaust gas recirculation (EGR) became a hot spot to achieve efficiency levels more similar to CI engines, while keeping traditional SI engine-out emission advantages [5,6]. Electric powertrains also come into play as a good solution to displace emissions from urban areas owing to a good promotion from public opinion, governments, and associations [7]. However, their lower power densities, higher production costs, as well as the real impact that these may have on ambience have limited up to now their market share [8,9]. For this reason, hybrid powertrains combining electrification with SI engines is currently seen as the most spread solution in the upcoming years. Nevertheless, their implementation implies new challenges for other emission control, since the vehicle operation in electrical mode can imply a delay in the engine and aftertreatment warm-up. Knorr et al. [10] found that the temperature drop in the exhaust line linked to engine shutdown in electrical mode is in the order of 150 $^{\circ}C$, so the catalyst may drop below the light-off temperature for the next engine start. This supports the increased emission observed in several other studies. In this way, Pham et al. [11] demonstrated high regulated emissions during high-powered cold starts. The results exceeded more than 9 times Federal Test Procedure (FTP) gaseous emissions for cold starts. As far as particulate matter is concerned, its emission from plug-in hybrid electric vehicles (PHEV) can be of the same order of magnitude as these from vehicles without any electrification [12]. The reason is found in the high number of high-powered engine starts through the driving cycle, as also concluded by Zinola et al. [13].

In this context, engine development for future electrified powertrains may need to take particular attention to emission control not only from the aftertreatment system perspective but also from the point of view of their formation inside the cylinder. In this sense, it is necessary to analyze the influence of the aforementioned technologies aimed at reducing engine fuel consumption, also looking at their impact on engine-out emissions. Particularly, the application of EGR can significantly modify the characteristics of the combustion process and the exhaust gas composition as well as further reduce the exhaust gas temperature. Some of these aspects are discussed next.

First, as it is well known, EGR was adopted in CI engines due to its capability to reduce raw NO_x emissions. This capability is well explained by the simplified Zeldovich mechanism [14,15], in which it is assumed that NO formation is in equilibrium. The basics are described in Equation (1),

$$\frac{d[NO]}{dt} = \left(\frac{6 \times 10^{16}}{T^{0.5}}\right) \cdot exp\left(\frac{-69096}{T}\right) \cdot [O_2]_e^{0.5} \cdot [N_2]_e \quad (1)$$

where $[NO]$ refers to the instantaneous molar concentration of NO, and $[O_2]_e$ and $[N_2]_e$ denote the equilibrium concentration of molecular oxygen and nitrogen, respectively. According to this expression, NO_x emissions, mainly composed of NO, depend on oxygen concentration and temperature. Therefore, a double effect occurs when introducing EGR into the cylinder:

1. **Thermal**: The exhaust gases are composed of a high proportion of H_2O and CO_2, which have a greater heat capacity than other air constituents, acting as a heat sink and reducing the temperature inside the cylinder during compression and combustion.
2. **Dilution**: The oxygen concentration is reduced as a result of the higher amount of inert gases inside the chamber, reducing the reactivity related to NO formation.

These effects have been studied in depth [16–18] resulting in a clear demonstration of NO_x reduction with O_2 concentration decay. However, the benefits of EGR implementation in SI engines can go beyond being only a NO_x inhibitor. As stated, the presence of exhaust gases with higher heat capacities acts as a heat sink, hence reducing in-cylinder temperature and heat transfer losses [19,20].

Furthermore, benefits at both partial and high loads are found. The need to increase the intake pressure to bring in exhaust gases along with fresh air is reflected in more open throttle positions and reduced pumping losses during throttled operation. In addition, using EGR allows better combustion phasing at higher loads, which is typically limited due to knock combustion phenomena [21]. Thanks the lower reactivity of the mixture knock probability is reduced, so the

spark control can be optimized, thus achieving better efficiencies [22]. Additionally, the temperature of the exhaust gases is also reduced as a combination of both effects (dilution plus more advanced phasing). Therefore, fuel enrichment commonly done at these high loads to protect the turbine from thermal fatigue [2,19,23] can be limited or completely suppressed, achieving further benefits from fuel consumption and emissions perspective.

Nevertheless, apart from the benefits achieved from fuel consumption perspective, EGR addition could negatively affect other emissions such as CO, Particle matter (PM), and Unburnt hydrocarbon (HC), as discussed by Gu et al. [24], or critically slow down flame development, producing unstable combustion and large cyclic variations, as shown by Galloni et al. [25]. Bermudez et al. [26] also proved the trend of HC increase with EGR use for all tested points due to reduction in combustion temperature and a greater quenching area.

Park et al. [27] studied the effects of combining EGR with stratified combustion as well as injection timing. The results showed the greater potential of EGR compared to retarded ignition timing on reducing harmful NO_x and HC emissions. Other studies have focused on analyzing and comparing cooled and uncooled EGR, finding out that cooled EGR normally shows more benefits than hot EGR from efficiency perspective [28], mainly thanks to an improved volumetric efficiency. However, cooled EGR results in a further reduction of NO_x emissions, whereas HC emissions and cycle-to-cycle variations deteriorate [15]. Furthermore, the usage of cooled EGR can be significantly limited by condensation issues either in the EGR cooler [29] or in the intercooler [30], reducing the potential impact of the EGR circuit, especially in hybrid electric vehicle applications, where temperature would significantly decrease when the powertrain runs in electric mode.

In summary, previous works highlight that EGR usage in spark-ignition engines can significantly alter the traditional composition of exhaust gases, at least reducing NO_x and increasing HC concentrations, and can reduce the exhaust gas temperature. This may further stress the operation of aftertreatment systems used in such applications, since traditional three-way catalysts depend on NO_x for HC and CO oxidation. Therefore, the current work intends to further assess the impact of EGR addition on engine-out emissions and to provide a preliminary evaluation about the potential oxidation performance of a purpose-made catalyst from a theoretical perspective. The investigation was done on a spray-guided spark-ignition engine including cooled low-pressure EGR, a variable valve-timing system (in both intake and exhaust camshafts), and a variable geometry turbine. In a first step, optimized calibrations from a fuel consumption perspective were generated at different levels of EGR using a design of experimental techniques at several steady-state keypoints. The design of experiments included variations of the EGR rate, the spark timing, and the settings of intake and exhaust variable valve timing system (VVT), maintaining approximately stoichiometric combustion. Then, these optimized calibrations were run in the engine to evaluate the impact of the EGR rate on engine-out emissions and oxygen content in the exhaust gases. Considering the new composition of the exhaust gases, mainly characterized by lower NO_x and oxygen content as well as high HC concentration, the potential capability of a catalyst to completely oxidize HC and CO emissions was evaluated from a theoretical stoichiometric analysis.

2. Materials and Methods

For this study, a four-stroke 1.3 L four cylinder, turbocharged, direct-injection spark-ignited engine was used. The main characteristics of the engine are highlighted in Table 1. This engine was also equipped with a variable geometry turbine technology (VGT). Thanks to a variable valve timing system (VVT), intake and exhaust actuations could also be delayed or advanced independently, maintaining the same valve lift and event duration, on a range of 40 crank angle degrees for both the intake and exhaust sides. When the corresponding variables in the engine control unit (ECU) were set to zero, the engine would operate in the minimum overlap condition, whereas values of forty would maximize the valve overlap (i.e., delaying the exhaust and advancing the intake valve profiles).

Table 1. Engine main characteristics.

Magnitude	Units	Value
Engine type	-	4-stroke, turbocharged
Number of cylinders	-	4
EGR circuit	-	Cooled low-pressure (LP)
Turbocharger	-	VGT
Displaced volume	cc	1300
Stroke	mm	81.2
Bore	mm	72
Compression ratio	-	10.6:1

A prototype low-pressure (LP)-EGR line was added to the original engine, extracting the gases after a commercial three-way catalyst. The line consists of an EGR cooler, an EGR valve downstream this cooler, and an intake valve located upstream the compressor, which allows for greater EGR flows when the pressure difference between intake and exhaust lines is low.

As generally adopted [15,26,31], the EGR rate is calculated from the CO_2 concentrations measured at the intake and exhaust lines:

$$EGR_{rate} = \frac{[CO_{2,int}] - [CO_{2,atm}]}{[CO_{2,exh}] - [CO_{2,atm}]} \times 100 \quad (2)$$

where $[CO_{2,int}]$ and $[CO_{2,exh}]$ represent the mole fraction of CO_2 at the intake and exhaust, respectively, whereas $[CO_{2,atm}]$ represents ambient mole fraction of CO_2. In particular, the intake CO_2 is sampled in the intake manifold, whereas the exhaust one is measured at the turbine outlet together with the rest of the exhaust emissions. Both are analyzed by means of a HORIBA MEXA-ONE system.

The test bench was controlled with AVL-PUMA software, allowing instantaneous speed and engine torque by means of a dynamometric brake AVL AFA 200/4-8EU. Besides, any modification of the intake and exhaust VVT system, the throttle valve position, and the spark timing were done via a partially opened ECU, which was equipped with an air flow meter to ensure proper lambda control when operating with EGR. The main ECU variables were registered through INCA v7.1. Instead, the VGT and EGR valves were controlled in open loop configuration independently from the ECU based on a National Instruments PXI system, previously described in [32]. The same system was used for high-frequency acquisition. For this purpose, instrumented spark-plugs (AVL ZI33) were mounted in all four cylinders in addition to the instantaneous intake and exhaust manifold pressures (Kistler 4007), measured in their respective manifolds. An AVL optical encoder was installed to provide a crank angle reference for instantaneous pressure measurements with a sampling of 0.2 crank angle degree. The instrumentation was completed with mean pressure and temperature acquisition in the most critical sections of the exhaust, intake, and cooling systems. Other magnitudes such as air and fuel mass flow (AVL FLOWSONIX and 733S, respectively) or the turbocharger speed (MICRO-EPSILON DS05) were also acquired. The engine layout is depicted in Figure 1.

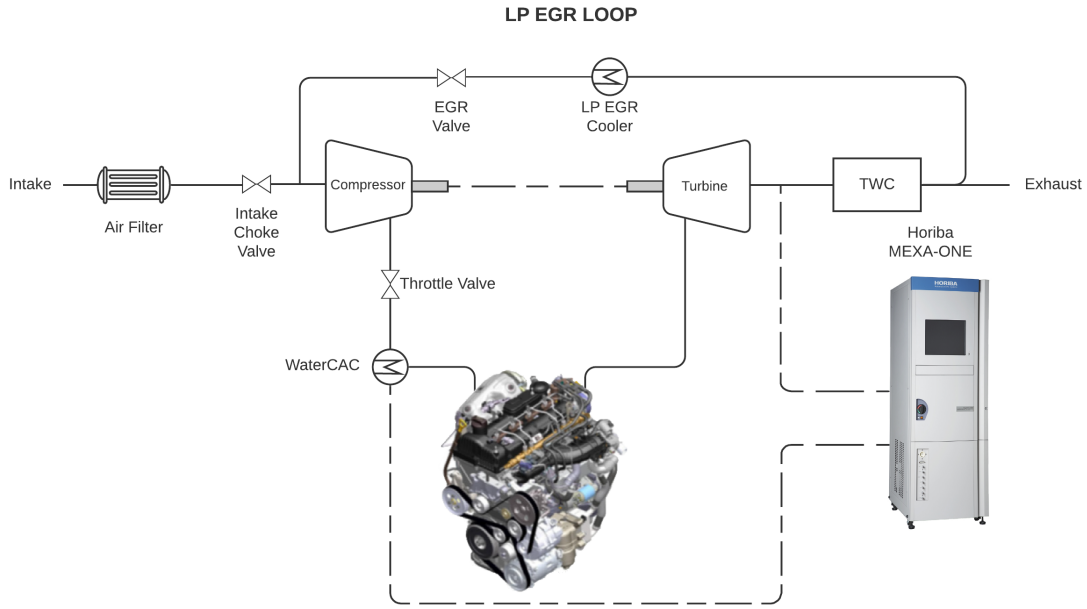

Figure 1. Engine setup diagram.

As stated in the introduction, the main objective of this study is to analyze the impact of different levels of EGR on the exhaust emissions of a turbocharged spark-ignition engine. However, these emissions will be affected not only by the EGR rate, but also by the spark timing (due to the impacts on combustion velocity and the temperature evolution inside the cylinder) and the VVT settings (since it controls the amount of internal residuals trapped inside the cylinder, especially at low loads). Therefore, in order to have a meaningful assessment of the exhaust emissions impact, it is necessary to have a proper combination of these calibration parameters as a function of the EGR rate. For this purpose, a design of experiments (DoE) was performed for six operating points, in a range from 1500 to 3000 revolutions per minute (rpm) and 6 to 15 bar of brake mean effective pressure (BMEP). This design of experiments was used to extract optimal calibrations at different levels of EGR, from zero to the maximum possible at each keypoint, aimed at optimizing the brake thermal efficiency. To successfully conduct the DoE, lower and upper boundaries had to be determined for each of the variables for every DoE. Intake and exhaust VVT boundaries were set according to safety limits to avoid contact between valves and the piston head. On the other hand, spark advance and EGR rate boundaries were set based on preliminary tests: at high loads, combinations of low EGR and advanced spark were excluded to avoid knocking combustion; at lower loads, combinations of high EGR and retarded spark actuation were also taken out to avoid excessive combustion instability and misfires. Finally, the throttle actuation or the VGT were used to establish the engine torque once the rest of the parameters were set. Table 2 shows the ranges covered for each keypoint, while Figure 2 shows an example of the configuration of the DoE for the engine point of 1500 rpm and 6 bar BMEP.

Table 2. Design of experiment (DoE) parameter definitions.

Engine Point rpm - bar	VVT Intake & Exhaust (°)	Spark Advance (° bTDC)	EGR Rate (%)
1500 - 6	0–40	10–35	0–28
1500 - 12	0–40	0–20	0–33
2000 - 6	0–40	5–35	0–28
2000 - 15	0–40	−5–25	0–32
2500 - 14	0–40	0–35	0–35
3000 - 12	0–40	3–32	0–25

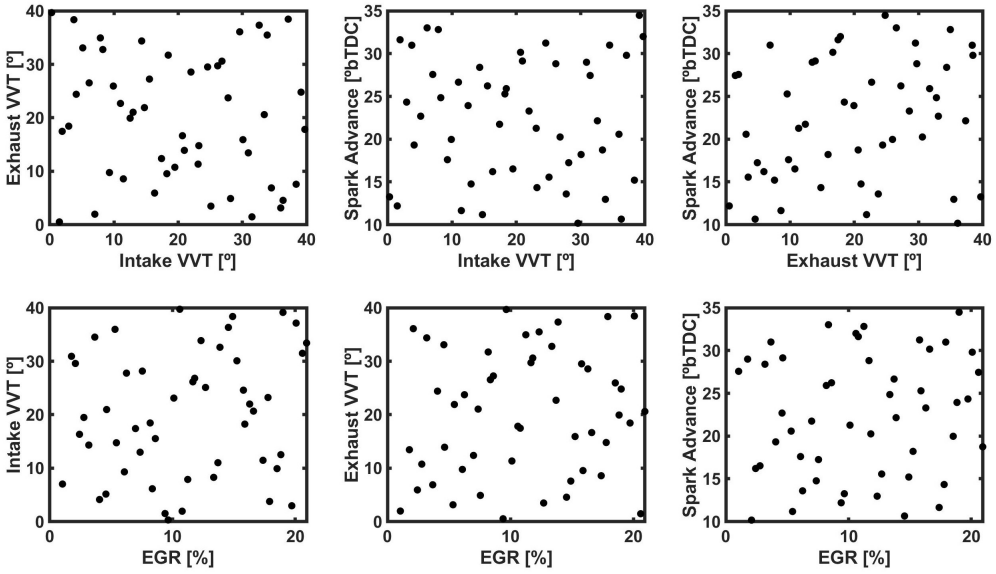

Figure 2. DoE test combinations for 1500 rpm 6 bar brake mean effective pressure (BMEP).

Once the DoE was completed and data were processed, every test must overcome two barriers: combustion stability and knock. If one of these limits was surpassed, the test was discarded before generating the surface response model. The combustion stability was defined in terms of a COV (coefficient of variance) limit for the indicated mean effective pressure (IMEP), set to 3.33% for the 6 bar BMEP points and 2.5% for the higher BMEPs. As widely accepted [22], COV of the IMEP was computed using information from a 200-cycle acquisition:

$$COV_{IMEP} = \frac{std(IMEP)}{mean(IMEP)} \times 100 \tag{3}$$

Knock intensity was assessed based on the MAPO (Maximum Amplitude of Pressure Oscillations) parameter. The method consists of in-cylinder pressure analysis using a high-pass filter to analyze oscillation in the time domain, calculating the maximum absolute value of the filtered pressure signal as stated by [32]. A maximum of 3% of a 200-cycle acquisition over a 0.5 bar limit was considered acceptable. This limit was established based on previous characterization of knocking cycles at the same engine speed.

A 1-D engine model based on GT-Power software, previously developed and validated by [33], was used in order to estimate the amount of residual gas trapped in the 6 bar BMEP operating points due to the high interaction between these residuals and the external EGR for analysis of the engine-out emissions. For a proper estimation of these residuals, it was necessary to have fine control of the intake and exhaust manifold conditions (pressure and temperature). For that purpose, the variable geometry turbine was controlled to match the experimental pressure in the exhaust manifold, while the temperature was achieved thanks to a heat transfer multiplier in the exhaust pipes. In the intake side, the compressor speed was set to obtain the experimental compressor outlet pressure. Then, depending on the operating condition, the engine's main throttle position was changed to achieve the experimental intake manifold pressure. Finally, the intake manifold temperature was controlled through the operation of the charge-air cooler.

Finally, the theoretical capability of a purpose-made catalyst to fully oxidize the HC and CO emissions under new boundary conditions in terms of temperature and exhaust gases composition was evaluated. For this purpose, a simple stoichiometric calculation is proposed:

$$\dot{m}_{O_2,req} = \left[\frac{1}{2}\frac{\dot{m}_{CO}}{MW_{CO}} + \left(n + \frac{m}{4}\right)\frac{\dot{m}_{HC}}{MW_{HC}} - \frac{1}{2}\frac{\dot{m}_{NO}}{MW_{NO}}\right] MW_{O_2} \tag{4}$$

where $\dot{m}_{O_2,req}$ is the mass flow of oxygen in the exhaust gases required to achieve a complete oxidation of HC and CO (assuming all NO is oxidized to NO_2, and this is reduced to N_2 in the subsequent HC/CO oxidation), $\dot{m}_i$ is the experimental mass flow of species i, MW_i is the molecular weight of the same component, and n and m are the number of carbon and hydrogen atoms of the unburned hydrocarbons composition. For this estimation, unburned hydrocarbons are represented by dimethylbutadiene (C_6H_{10}) for all the conditions, based on a previous speciation of the exhaust gases.

3. Results and Discussion

In this section, the main results in the analysis of exhaust emissions will be presented. In order to synthesize these results, two keypoints representative of medium and low engine load operation were selected. The reason for this distinction is the different behaviors in terms of internal residuals: while in the turbocharged area (approximately equal or higher than 10 bar BMEP) the amount of internal residuals is not very sensitive to the variation of the valve timings, in throttled operation, the VVT settings induce significant variation of the engine trapping ratio (and therefore internal residuals). Since both internal residuals and exhaust gas recirculation can produce similar results in terms of thermal NO_x production as well as laminar flame speed characteristics (linked to unburned hydrocarbons), these conditions need to be treated separately.

3.1. Medium Load: 3000 rpm - 12 bar BMEP

Figure 3 shows the calibration produced by the DoE methodology as a function of the EGR rate. As previously mentioned, VVT settings at 0–0 represent the minimum overlap condition, which is in this case the optimal before EGR is introduced. Instead, when EGR is introduced, the exhaust valve timing is maintained but the intake valve opening is anticipated. Additionally, the spark timing is severely anticipated as a consequence of two phenomena: the reduction of knock probability and the slower flame propagation characteristics.

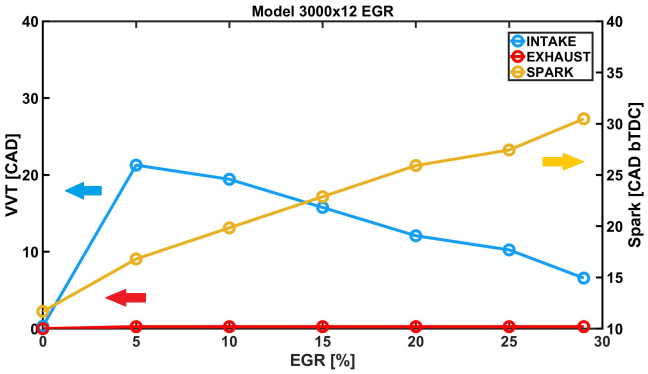

Figure 3. Engine calibration achieved by the DoE for 3000 rpm and 12 bar BMEP.

The results obtained in terms of emissions are depicted in Figure 4. The data are presented in terms of the variation produced with respect to the calibration without EGR using the data extracted from the gas analyzer measurement in mole fraction. The most direct and clear result is the one corresponding to NO_x emissions (upper left chart). As stated in the introduction, the combination of lower oxygen concentration and higher heat capacity in the unburned region as a consequence of EGR introduction results in a reduction of NO formation according to the Zeldovich mechanism. The unburned hydrocarbon (lower left graph) trend instead is mostly related to the quenching phenomena. As the EGR rate increases, laminar flame speed is deteriorated, which can be confirmed by the increase in the induction time reflected in the same graph. This induction time is defined as the lapse between the spark activation and 10% of the cumulative heat released, related to the initial kernel growth which is known to be greatly influenced by laminar flame speed as well as flow characteristics around the spark plug [34]. Regarding the oxygen content in the exhaust gases (upper right figure), it has to be highlighted that, since the engine is always running at stoichiometric

conditions, this oxygen is significantly influenced by the aforementioned quenching phenomena. On the one hand, as quenching distance increases, the volume of fresh mixture existing in the exhaust gases is higher, so higher oxygen levels could be expected. However, with the increase of the EGR rate, the oxygen concentration inside this fresh mixture is lower, driving the continuous reduction of oxygen concentration found in the results.

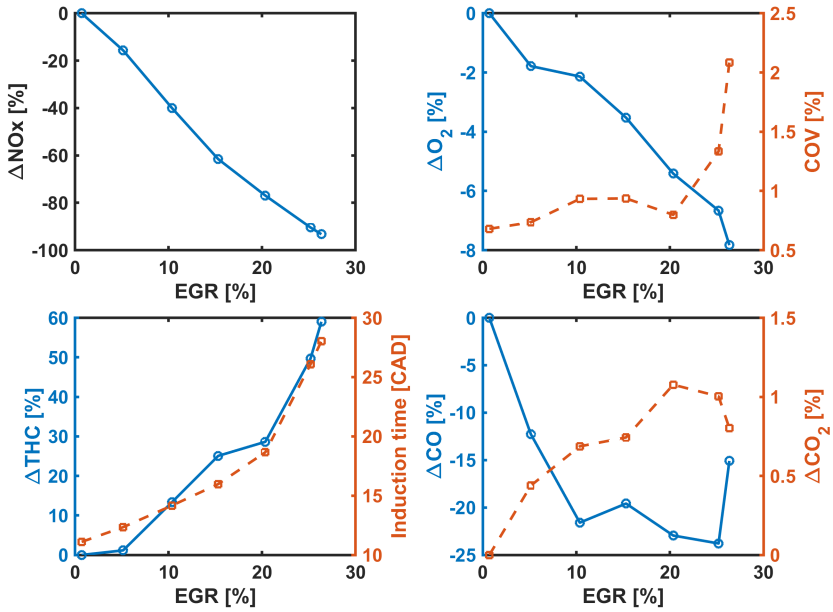

Figure 4. Engine-out emissions as a function of the exhaust gas recirculation (EGR) rate for 3000 rpm and 12 bar BMEP.

More complex is the evolution of the CO emissions (lower right graph). In general, CO concentration in the exhaust is governed by the kinetics of the oxidation reaction of CO to CO_2 in the last stages of the combustion process, as it can be seen from the inverse trend shown by the CO_2 in the same plot. In principle, the reduction of oxygen concentration when increasing the EGR rate implies that thermal equilibrium of that reaction would be shifted towards a higher concentration of CO. However, there are two phenomena opposite to that trend. On the one hand, reduction of the combustion temperature reduces the dissociation of CO_2 once it is formed. On the other hand, the kinetics of the reaction are slowed down. Nevertheless, it has to be considered that there is a severe interaction between these aspects and the evolution of the combustion process due to the instantaneous temperature evolution inside the cylinder, so changes in the spark timing and/or the variable valve timing settings may also influence the CO trend. Finally, it has to be considered that, at very high EGR rates, the combustion stability is deteriorated, as it can be observed in the COV of the IMEP, which is plotted with the oxygen concentration (upper right side), producing an increase of CO emissions compared to the general trend achieved with EGR.

As a conclusion from the previous results, high external EGR operation induces exhaust gases with very low oxygen and NO_x while unburned hydrocarbons increase and CO decrease but to a lesser extent. These new conditions in terms of exhaust gas composition would induce difficulties to achieve a complete oxidation of HC and CO for a traditional three-way catalyst, such as the one present in the current experimental setup, which depends on NO_x for CO abatement. Therefore, analyzing the conversion efficiency in that catalyst would not provide a realistic assessment. Instead, a new catalyst design targeted for these new conditions should be proposed. With that in mind, the theoretical evaluation based on stoichiometric considerations presented in Section 2 was employed to analyze the potential capability of an ideal catalyst to achieve a complete oxidation of HC and CO. Figure 5 shows the result of the application of the catalyst stoichiometric model to the results previously seen. In this chart, the cumulative O_2 mass during the 60 s acquisition performed during the test is compared to the

amount of oxygen that would be required to achieve a complete oxidation of HC and CO, according to Equation (4). Additionally, the value of lambda obtained from the experimental air and fuel mass flows is included. As it can be seen, at low EGR rates, the oxygen available is more than enough to produce complete oxidation of the emissions. However, as EGR increases, the increase in HC and the reduction of NO_x produce results in which the margin of oxygen available is reduced. In part, the fact that the oxygen content arriving at the catalyst is still enough to produce results in which full oxidation of the HC emissions is linked to the reduction of raw CO, which partially compensates the lack of oxygen. For the highest level of EGR, the CO tends to increase again, reaching a condition where the oxygen available is practically equal to the one theoretically necessary. Considering this result, a slightly lean condition is probably advisable for very high EGR rates, especially considering the significant reduction of engine out NO_x that can be achieved thanks to the addition of EGR. However, it has to be considered that, in this case, the low margin in exhaust oxygen is partially produced by the slightly rich lambda achieved in these conditions.

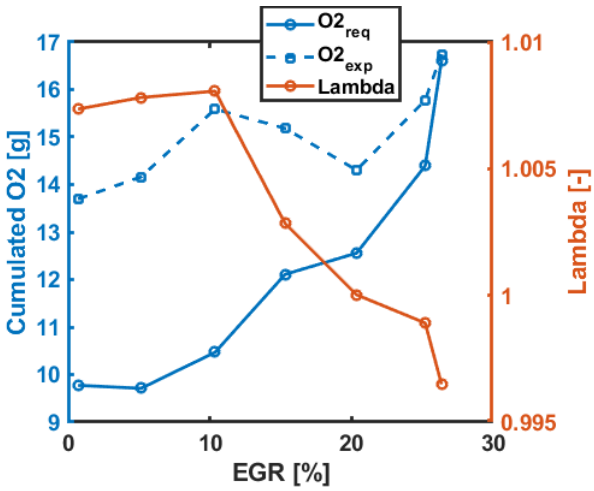

Figure 5. Catalyst performance extrapolation for 3000 rpm and 12 bar BMEP.

3.2. Low Load: 1500 rpm - 6 bar BMEP

In the case of 1500 rpm 6 bar BMEP, the engine performance is determined by the fact that the load is controlled by the throttle operation. Therefore, when using the same methodology previously explained, optimization of the DoE tends to produce calibrations with the highest possible overlap (VVT 40–40) to reduce the pumping losses.

This reduction is produced by the higher amount of internal residuals trapped at the valve closures and greater throttle positions, as it can be seen in Figure 6, where maximum values of residuals up to 25% can be achieved when the engine operates in this condition compared to around 5% when minimum overlap is set (VVT 0–0). The reduction of the maximum amount of internal residuals achieved when the external EGR rate increases is related to the lower pressure difference across the engine (between intake and exhaust manifolds), since a higher amount of EGR is linked to higher intake manifold pressure to achieve the same engine load.

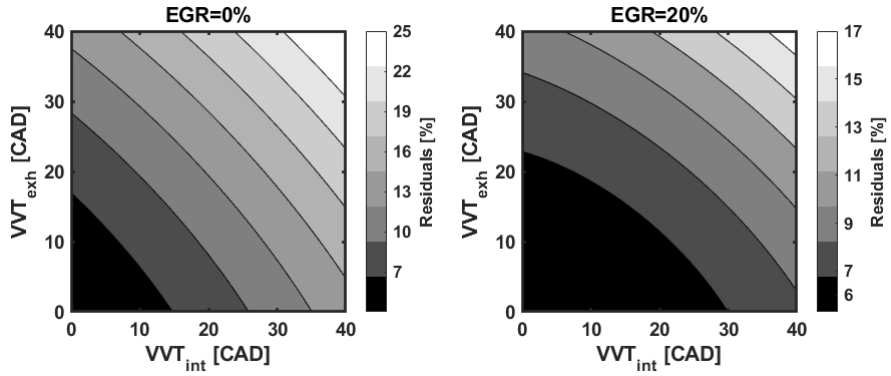

Figure 6. Residuals prediction as a function of variable valve timing system (VVT) settings for 1500 rpm and 6 bar BMEP. **left**: no EGR; **right**: 20% EGR.

The lower residual concentration found with smallest possible overlap (VVT 0–0) is also translated into the possibility of increasing the EGR rate compared to higher overlap, and the benefit is seen in gross indicated efficiency probably due to lower heat losses. This can be observed in Figure 7, where two EGR sweeps are shown, one at maximum overlap (blue) and the other at minimum overlap (orange).

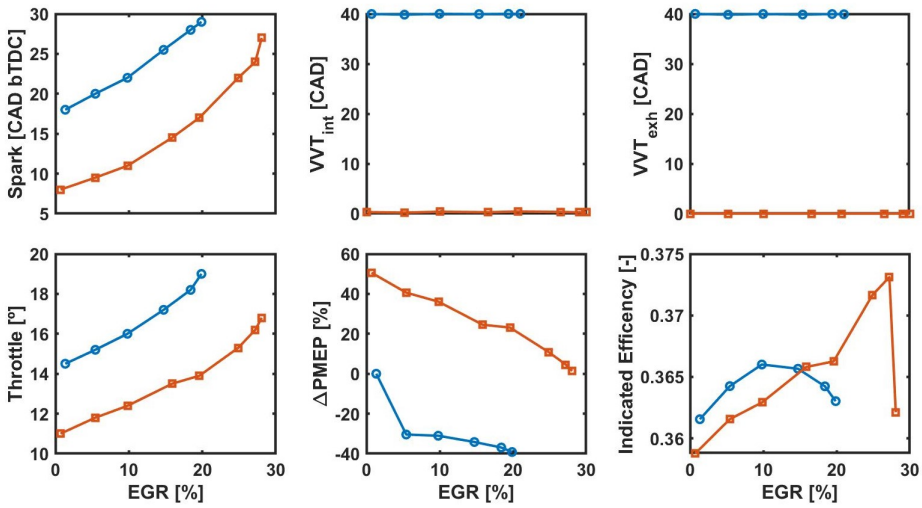

Figure 7. EGR sweeps with different VVT settings for 1500 rpm and 6 bar BMEP. Maximum overlap: blue; minimum overlap: orange.

The results of the EGR variation for the maximum overlap condition in terms of emissions are depicted in Figure 8. The data are presented using the same organization as already described for the medium load operating point. Again, NO_x emissions (upper left chart) are directly driven by the lower temperature and oxygen content of the unburned zone inside the cylinder. Unburned hydrocarbon (lower left graph) results are mostly linked to the impact of EGR on flame propagation characteristics, as highlighted by the higher induction time. Regarding the oxygen content available in the exhaust gases, different results are achieved depending on the EGR range. Initially, up to 10% EGR, the oxygen content was almost independent on the EGR rate, contrary to the continuous reduction seen in the medium load operating condition. This can be partially explained by the interaction with the internal residuals. While in the medium load conditions these residuals are not very significant and therefore the oxygen content is directly linked to the external EGR, in the case of the low load operation, the oxygen content is severely affected by these residuals. As previously seen, as the EGR rate increases, the amount of internal residuals is reduced due to the effect on the pressure differential

across the engine, compensating the trend in terms of oxygen concentration in the unburned mixture. Therefore, it is not until the external EGR is increased up to 15% that the decrease of the oxygen content can be observed. However, from this point on, there is a severe combustion stability deterioration, more critical than the one observed at higher load due to the combination of high internal residuals and external EGR, leading to a new increase of O_2 concentration. This evolution affects the CO-CO_2 kinetics, summarized in the lower right plot of Figure 8.

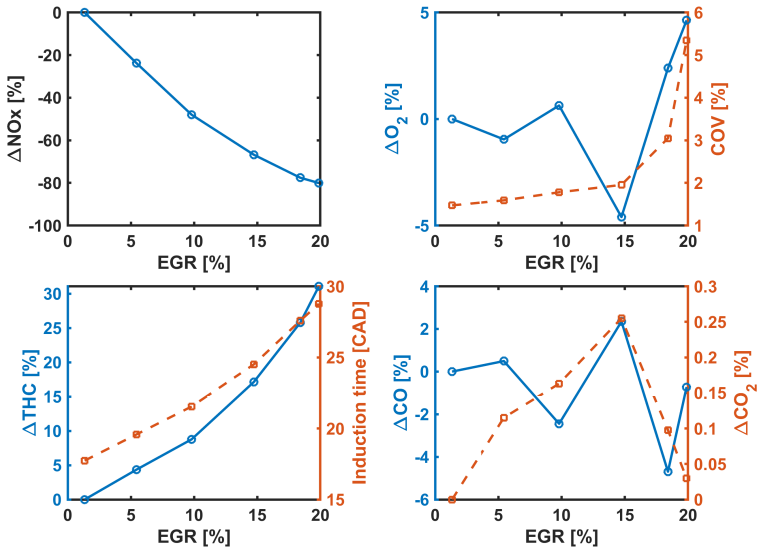

Figure 8. Engine-out emissions as a function of the EGR rate for 1500 rpm and 6 bar BMEP for the maximum valve overlap condition.

Due to the interaction of the emissions result with the internal residuals, it is also interesting to analyze what would be the result if the engine was run at minimum overlap condition. This information is depicted as continuous lines in Figure 9 and compared to the previous results with maximum overlap, represented in dashed lines. In all cases, the datum to calculate the variations of emissions is the condition with no external EGR and maximum valve overlap (i.e., the no EGR condition from the previous graph). The most evident difference between both datasets is the range itself of external EGR that can be added by maintaining stable combustion. While previously a deterioration in the coefficient of variation of the IMEP could be observed from 15% EGR, a reduction of the internal residuals allows the EGR to increase up to 25% before any impact on combustion instability can be detected. In terms of NO_x, it is clear how running the engine without external EGR or internal residuals results in a huge increase of these emissions. Actually, it can be seen how the level of NO_x only with internal residuals is not reached until adding around 25% EGR, which is consistent with the residual prediction achieved with GT-Power for the maximum overlap condition, previously depicted in Figure 6. Regarding unburned hydrocarbons, the reduction of internal residuals results in a faster flame propagation (lower induction time) and consequently lower emissions, but the slope of increase with the addition of external EGR is similar for both VVT settings. Moreover, the reduced amount of residuals implies that the oxygen concentration achieves a monotonous reduction as a function of EGR until unstable combustion operation is reached, similar to what was already discussed for medium load conditions, compared to the almost flat behavior seen with maximum overlap. Furthermore, the oxygen availability is always lower than in the case of the maximum overlap condition, as a consequence of the lower quenching distance and therefore lower volume in the unburned zone at the end of combustion. Adding external EGR with minimum overlap induces a reduction of CO, and an increase of CO_2 is also observed, while the results are similar in CO and slightly lower in CO_2 compared to the high overlap operation at similar total residuals. Therefore, it can be concluded that

the effect of EGR on exhaust emissions is not so much affected by the different engine operating point but more about the interaction with the internal residuals through the VVT.

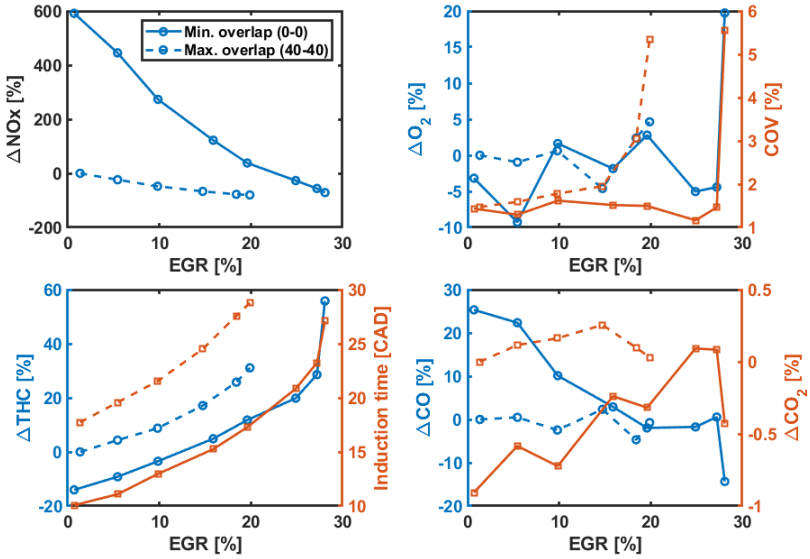

Figure 9. Engine-out emissions as a function of the EGR rate for 1500 rpm and 6 bar BMEP. Continuous lines: minimum overlap; dashed lines: maximum overlap.

Figures 10 and 11 show the prediction of the required O_2 to completely abate CO and HC emissions in the catalyst for the high and low valve overlap conditions, respectively. As it can be seen, in both cases, the cumulated oxygen available in the exhaust is higher than the one required theoretically to completely oxidize HC and CO. However, slight differences are observed depending on the valve overlap conditions. In the case of the low overlap condition, the margin between available and required oxygen is reduced as the EGR rate increases, which is similar to the trend already described in the 3000 rpm medium load keypoint. The main difference is that, in this case, the equivalence ratio control results in a slightly lean mixture for all conditions, while in the medium load case, the mixture was slightly rich for the highest EGR point, affecting oxygen availability. Instead, for the high overlap condition, the margin is similar for the whole EGR range considered. This behavior is mostly due to the low sensitivity previously seen for CO and oxygen content in the exhaust gases when increasing EGR in the maximum valve overlap case.

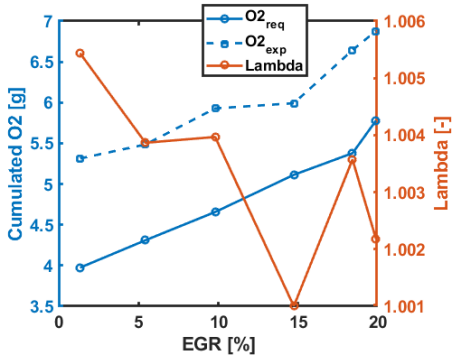

Figure 10. Catalyst performance estimation for 1500 rpm and 6 bar BMEP: high valve overlap conditions.

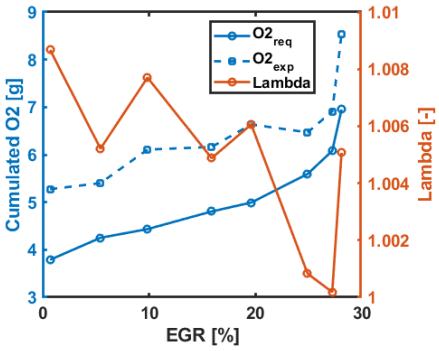

Figure 11. Catalyst performance estimation for 1500 rpm and 6 bar BMEP: low valve overlap conditions.

3.3. Overall Assessment

Table 3 includes a summary of the emissions impact found for all six operating points described in Section 2. In particular, the values obtained in terms of NO_x, CO, and HC are provided for the no EGR condition as well as for the maximum EGR rate run in the study. Additionally, in the case of the 1500 rpm 6 bar BMEP condition, the results are provided for the two valve overlap settings previously discussed.

The first three rows correspond to the low engine load condition, analyzed for both 1500 and 2000 rpm. In the case of 2000 rpm 6 bar BMEP, it has to be considered that the calibration optimization provided high overlap settings for the no EGR case and low overlap when the maximum rate was applied. Therefore, the amount of internal residuals helps to maintain relatively low NO_x already without external EGR, but even greater potential to reduce this emission is achieved with cooled EGR thanks to the lower initial temperature reached inside the cylinder. Other than that, similar increases in HC and decreases in CO as already discussed for the 1500 rpm condition are observed. The maximum EGR rate reachable with minimum overlap is also consistent between both conditions.

The last raws show the results for the medium load points, ranging from 12 to 15 bar BMEP depending on the engine speed. In this case, the amount of internal residuals is always low regardless of the VVT settings employed, so the results are more similar to the condition of minimum overlap seen in the low-load region. Therefore, the impact of external EGR on NO_x is more severe, being reduced around one order of magnitude for all conditions. Additionally, the CO emissions are reduced to a lesser extent, stressing more the catalyst capabilities as already discussed for the 3000 rpm 14 bar BMEP condition.

Table 3. Emission comparison between zero EGR and maximum EGR operation.

Engine Point rpm - bar	EGR (%)	NO_x (ppm)	HC (ppm)	CO (ppm)
1500 - 6 bar (max. overlap)	0	401	2306	5938
	19.9	80	3023	5895
1500 - 6 bar (min. overlap)	0	2777	1982	7442
	28.0	116	2965	5087
2000 - 6 bar	0	1006	1926	6988
	27.7	155	2687	5171
1500 - 12 bar	0	2645	1366	6306
	24.6	392	1987	5162
2000 - 15 bar	0	2764	1230	8158
	27.4	185	1700	7592
2500 - 14 bar	0	3359	1138	5271
	28.8	187	1821	5200
3000 - 12 bar	0	3240	1196	6310
	26.3	218	1902	5358

4. Conclusions

In the current paper, an investigation of the effects of usage of exhaust gas recirculation on a spark-ignition engine-out emissions is presented. For this purpose, a 4-cylinder turbocharged Gasoline direct injection (GDI) engine equipped with VVT, VGT, and a low-pressure EGR line was used. In order to have a meaningful assessment of these emissions, the engine had been previously calibrated for 6 engine operating points varying speed and load and for different levels of EGR using the DoE technique, trying to always maintain stoichiometric conditions. Then, the found calibrations were run on the engine to assess the effect of increasing EGR quantity on emissions. Finally, a stoichiometric-based model of the reactions in the catalyst was used to evaluate the potential impact of the NO_x reduction and the HC increase with EGR on the catalyst performance. Doing so, the following conclusions have been found:

- In general, an approximately linear decay of NO_x and increase of HC is found as a function of the addition of external EGR, according to the expectations. On the one hand, NO_x is driven by the reduction of both the maximum combustion temperature as well as the oxygen availability in the unburned zone. On the other hand, the reduction of the flame propagation speed linked to this lower oxygen concentration, together with the lower rate of heat transfer to the cylinder walls, results in a higher quenching distance, increasing unburned HC.
- In terms of the oxygen concentration in the exhaust gases, which can be of interest for the catalyst operation, different trends are found depending on how the engine is controlled in terms of the VVT system. When the amount of internal residuals trapped in the cylinder is small, the lower oxygen concentration in the unburned zone (which will be transfered in the exhaust gases through quenching in the walls and crevices) when increasing EGR dominates over the increase in the quenching distance, inducing a reduction of the oxygen content seen in the exhaust. Contrarily, when the amount of these internal residuals increases (at low speed and load with high valve overlap), the effect of external EGR on the oxygen concentration in the unburned zone is smaller, since the addition of external EGR results in lower internal residuals due to the increase in intake manifold pressure, partially compensating the presence of external EGR and inducing an almost flat trend in CO and oxygen. However, when the amount of internal residuals plus external EGR is excessive, combustion instability appears, inducing cycles with low combustion efficiency and a significant increase of oxygen concentration in the exhaust.
- Regarding CO, the general trend is to reduce them when increasing EGR as a consequence of kinetic effects on the dissociation reaction of CO_2 but to a lesser extent than the increase in HC emissions previously observed.
- In general, despite the reduction of oxygen concentration and nitrogen oxides in the exhaust gases when increasing EGR, the oxygen available is still theoretically enough to produce a complete oxidation in the catalyst. This is in part thanks to the reduction of CO induced as EGR increases. However, for very high levels of EGR, the margin available in the oxygen amount is very small, especially when combustion stability deteriorates. Therefore, strategies with slightly lean operation may be needed in such conditions in order to ensure a robust response of the aftertreatment if the EGR rate is high enough to tolerate a small deterioration of NO_x conversion efficiency.

Author Contributions: Conceptualization, J.D.l.M.; formal analysis, E.J.S. and R.P.; funding acquisition, J.D.l.M. and P.P.; investigation, P.P., J.D.l.M., E.J.S., and R.P.; methodology, J.D.l.M. and P.P.; project administration, J.D.l.M.; software, P.P. and E.J.S.; supervision, P.P. and J.D.l.M.; writing—original draft, J.D.l.M. and R.P.; writing—review and editing, P.P., J.D.l.M., E.J.S., and R.P. All authors have read and agreed to the published version of the manuscript.

Funding: This research received no external funding.

Acknowledgments: The authors would like to thank Mr. Vicente Esteve for his valuable collaboration during the experimental work.

Conflicts of Interest: The authors declare no conflict of interest. The founding sponsors had no role in the design of the study; in the collection, analyses, or interpretation of data; in the writing of the manuscript; or in the decision to publish the results.

Abbreviations

BMEP	Break mean effective pressure
bTDC	Before top dead center
BSFC	Brake specific fuel consumption
CI	Compression ignition
CO	Carbon monoxide
CO_2	Carbon dioxide
COV	Coefficient of variation
DoE	Design of experiments
ECU	Electronic control unit
EGR	Exhaust gas recirculation
HC	Unburnt hydrocarbon
H_2O	Water
GDI	Gasoline direct injection
IGR	Internal gas recirculation
IMEP	Indicated mean effective pressure
LHV_i	Lower heating value of species i
LP-EGR	Low-Pressure EGR
m	Number of carbon atoms of unburned hydrocarbons
$\dot{m}_i$	Mass flow of species i
MAPO	Maximum Amplitude of Pressure Oscillation
MW_i	Molecular weight of species i
n	Number of hydrogen atoms of unburned hydrocarbons
N_2	Nitrogen
NO	Nitrogen monoxide
NO_x	Nitrogen oxides
O_2	Oxygen
PFI	Port fuel injection
PHEV	Plug-in hybrid electric vehicle
PM	Particle matter
rpm	Revolutions per minute
SI	Spark ignition
TWC	Three-way catalyst
VGT	Variable geometry turbine
VVT	Variable valve timing
X_i	Mole fraction of species i

References

1. Kolodziej, C.P.; Pamminger, M.; Sevik, J.; Wallner, T.; Wagnon, S.W.; Pitz, W.J. Effects of Fuel Laminar Flame Speed Compared to Engine Tumble Ratio, Ignition Energy, and Injection Strategy on Lean and EGR Dilute Spark Ignition Combustion. *SAE Int. J. Fuels Lubr.* **2017**, *10*, 82–94. [CrossRef]
2. Sjerić, M.; Taritaš, I.; Tomić, R.; Blažić, M.; Kozarac, D.; Lulić, Z. Efficiency improvement of a spark-ignition engine at full load conditions using exhaust gas recirculation and variable geometry turbocharger—Numerical study. *Energy Convers. Manag.* **2016**, *125*, 26–39. [CrossRef]
3. Pinterits, M. *EU National Greenhouse Gas Inventory Report May 2014*; Number 09; European Environment Agency: Brussels, Belgium, 2014.
4. Grover, R.O., Jr.; Cleary, D. *Correlating Measured Combustion Performance with CFD Predicted In-Cylinder Flows for a Spark-Ignition Direct-Injection (SIDI) Engine with Enhanced Charge Motion*; SAE Technical Papers 2013-01-1090; SAE International: Detroit, MI, USA, 2013. [CrossRef]

5. Costa, M.; Catapano, F.; Sementa, P.; Sorge, U.; Vaglieco, B.M. Mixture preparation and combustion in a GDI engine under stoichiometric or lean charge: An experimental and numerical study on an optically accessible engine. *Appl. Energy* **2016**, *180*, 86–103. [CrossRef]
6. Alagumalai, A. Internal combustion engines: Progress and prospects. *Renew. Sustain. Energy Rev.* **2014**, *38*, 561–571. [CrossRef]
7. Dong, X.; Wang, B.; Yip, H.L.; Chan, Q.N. CO_2 Emission of Electric and Gasoline Vehicles under Various Road Conditions for China, Japan, Europe and World Average—Prediction through Year 2040. *Appl. Sci.* **2019**, *9*, 2295. [CrossRef]
8. Vafamehr, H.; Cairns, A.; Sampson, O.; Koupaie, M.M. The competing chemical and physical effects of transient fuel enrichment on heavy knock in an optical spark ignition engine. *Appl. Energy* **2016**, *179*, 687–697. [CrossRef]
9. Gröger, O.; Gasteiger, H.A.; Suchsland, J.P. Review—Electromobility: Batteries or Fuel Cells? *J. Electrochem. Soc.* **2015**, *163*, A2605–A2622. [CrossRef]
10. Knorr, T.; Ellmer, D.; Baensch, S.; Schatz, A. Optimization of the 48 V Hybrid Technology to Minimize Local Emissions in the RDE. In *27th Aachen Colloquium Automobile and Engine Technology*; Institute for Combustion Engines, RTWH Aachen University: Aachen, Germany, 2018.
11. Pham, A.; Jeftic, M. *Characterization of Gaseous Emissions from Blended Plug-In Hybrid Electric Vehicles during High-Power Cold-Starts*; SAE Technical Papers 2018-01-0428; SAE International: Detroit, MI, USA, 2018; pp. 1–9. [CrossRef]
12. Yamada, H.; Inomata, S.; Tanimoto, H. Particle and VOC Emissions from Stoichiometric Gasoline Direct Injection Vehicles and Correlation Between Particle Number and Mass Emissions. *Emiss. Control Sci. Technol.* **2017**, *3*, 135–141. [CrossRef]
13. Zinola, S.; Raux, S.; M, L. *Persistent Particle Number Emissions Sources at the Tailpipe of Combustion Engines*; SAE Technical Papers 2016-01-2283; SAE International: Detroit, MI, USA, 2016; pp. 1–10. [CrossRef]
14. Xie, F.; Li, X.; Su, Y.; Hong, W.; Jiang, B.; Han, L. Influence of air and EGR dilutions on improving performance of a high compression ratio spark-ignition engine fueled with methanol at light load. *Appl. Therm. Eng.* **2016**, *94*, 559–567. [CrossRef]
15. Wei, H.; Zhu, T.; Shu, G.; Tan, L.; Wang, Y. Gasoline engine exhaust gas recirculation—A review. *Appl. Energy* **2012**, *99*, 534–544. [CrossRef]
16. Ghazikhani, M.; Feyz, M.E.; Joharchi, A. Experimental investigation of the Exhaust Gas Recirculation effects on irreversibility and Brake Specific Fuel Consumption of indirect injection diesel engines. *Appl. Therm. Eng.* **2010**, *30*, 1711–1718. [CrossRef]
17. Al-Qurashi, K.; Lueking, A.D.; Boehman, A.L. The deconvolution of the thermal, dilution, and chemical effects of exhaust gas recirculation (EGR) on the reactivity of engine and flame soot. *Combust. Flame* **2011**, *158*, 1696–1704. [CrossRef]
18. Ladommatos, N.; Abdelhalim, S.M.; Zhao, H.; Hu, Z. *Effects of EGR on Heat Release in Diesel Combustion*; SAE Technical Papers 980184; SAE International: Detroit, MI, USA, 1998. [CrossRef]
19. Li, T.; Wu, D.; Xu, M. Thermodynamic analysis of EGR effects on the first and second law efficiencies of a boosted spark-ignited direct-injection gasoline engine. *Energy Convers. Manag.* **2013**, *70*, 130–138. [CrossRef]
20. Roy, M.M.; Tomita, E.; Kawahara, N.; Harada, Y.; Sakane, A. Comparison of performance and emissions of a supercharged dual-fuel engine fueled by hydrogen and hydrogen-containing gaseous fuels. *Int. J. Hydrogen Energy* **2011**, *36*, 7339–7352. [CrossRef]
21. Wang, X.; Zhang, X.; Wang, M.; Han, Y.; Chen, H. Numerical Simulation of Knock Combustion in a Downsizing Turbocharged Gasoline Direct Injection Engine. *Appl. Sci.* **2019**, *9*, 4133. [CrossRef]
22. Caton, J.A. The thermodynamic characteristics of high efficiency, internal-combustion engines. *Energy Convers. Manag.* **2012**, *58*, 84–93. [CrossRef]
23. Su, J.; Xu, M.; Li, T.; Gao, Y.; Wang, J. Combined effects of cooled EGR and a higher geometric compression ratio on thermal efficiency improvement of a downsized boosted spark-ignition direct-injection engine. *Energy Convers. Manag.* **2014**, *78*, 65–73. [CrossRef]
24. Gu, X.; Huang, Z.; Cai, J.; Gong, J.; Wu, X.; Lee, C.F. Emission characteristics of a spark-ignition engine fuelled with gasoline-n-butanol blends in combination with EGR. *Fuel* **2012**, *93*, 611–617. [CrossRef]
25. Galloni, E. Analyses about parameters that affect cyclic variation in a spark ignition engine. *Appl. Therm. Eng.* **2009**, *29*, 1131–1137. [CrossRef]

26. Bermúdez, V.; Lujan, J.M.; Climent, H.; Campos, D. Assessment of pollutants emission and aftertreatment efficiency in a GTDi engine including cooled LP-EGR system under different steady-state operating conditions. *Appl. Energy* **2015**, *158*, 459–473. [CrossRef]
27. Park, C.; Kim, S.; Kim, H.; Moriyoshi, Y. Stratified lean combustion characteristics of a spray-guided combustion system in a gasoline direct injection engine. *Energy* **2012**, *41*, 401–407. [CrossRef]
28. Tomazic, D.; Pfeifer, A. *Cooled EGR—A Must or an Option for 2002 / 04 Reprinted From : Compression Ignition Combustion and In-Cylinder Diesel Particulates and NO_x Control*; SAE Technical Papers 2002-01-00962; SAE International: Detroit, MI, USA, 2002.
29. Galindo, J.; Navarro, R.; Tarí, D.; Moya, F. Development of an experimental test bench and a psychrometric model for assessing condensation on a low-pressure exhaust gas recirculation cooler. *Int. J. Engine Res.* **2020**. [CrossRef]
30. Luján, J.M.; Dolz, V.; Monsalve-Serrano, J.; Maldonado, M.A.B. High-pressure exhaust gas recirculation line condensation model of an internal combustion diesel engine operating at cold conditions. *Int. J. Engine Res.* **2019**. [CrossRef]
31. Boccardi, S.; Catapano, F.; Costa, M.; Sementa, P.; Sorge, U.; Vaglieco, B.M. Optimization of a GDI engine operation in the absence of knocking through numerical 1D and 3D modeling. *Adv. Eng. Softw.* **2016**, *95*, 38–58. [CrossRef]
32. Pla, B.; De La Morena, J.; Bares, P.; Jiménez, I. *Knock Analysis in the Crank Angle Domain for Low-Knocking Cycles Detection*; SAE Technical Papers 2020-01-0549; SAE International: Detroit, MI, USA, 2020; pp. 1–11. [CrossRef]
33. Serrano, J.R.; Climent, H.; Navarro, R.; González-Domínguez, D. *Methodology to Standardize and Improve the Calibration Process of a 1D Model of a GTDI Engine*; SAE Technical Papers 2020-01-1008; SAE International: Detroit, MI, USA, 2020; pp. 1–13. [CrossRef]
34. Nishiyama, A.; Le, M.K.; Furui, T.; Ikeda, Y. The Relationship between In-Cylinder Flow-Field near Spark Plug Areas, the Spark Behavior, and the Combustion Performance inside an Optical S.I. Engine. *Appl. Sci.* **2019**, *9*, 1545. [CrossRef]